Effect of iron content and potassium substitution in A_{0.8}Fe_{1.6}Se_{2} (A=K, Rb, Tl) superconductors: A Raman scattering investigation

A. M. Zhang, K. Liu, J. B. He, D. M. Wang, G. F. Chen, B. Normand, and Q. M. Zhang

Phys. Rev. B **86**, 134502 — Published 1 October 2012

DOI: 10.1103/PhysRevB.86.134502

Effect of iron content and potassium substitution in $A_{0.8}Fe_{1.6}Se_2$ (A = K, Rb, Tl) superconductors: a Raman-scattering investigation

A. M. Zhang, K. Liu, J. B. He, D. M. Wang, G. F. Chen, B. Normand and Q. M. Zhang*
Department of Physics, Renmin University of China, Beijing 100872, P. R. China

We have performed Raman-scattering measurements on high-quality single crystals of the superconductors $K_{0.8}Fe_{1.6}Se_2$ (T_c = 32 K), $Tl_{0.5}K_{0.3}Fe_{1.6}Se_2$ (T_c = 29 K), and $Tl_{0.5}Rb_{0.3}Fe_{1.6}Se_2$ (T_c = 31 K), as well as of the insulating compound $KFe_{1.5}Se_2$. To interpret our results, we have made first-principles calculations for the phonon modes in the ordered iron-vacancy structure of $K_{0.8}Fe_{1.6}Se_2$. The modes we observe can be assigned very well from our symmetry analysis and calculations, allowing us to compare Raman-active phonons in the AFeSe compounds. We find a clear frequency difference in most phonon modes between the superconducting and non-superconducting potassium crystals, indicating the fundamental influence of iron content. By contrast, substitution of K by Tl or Rb in $A_{0.8}Fe_{1.6}Se_2$ causes no substantial frequency shift for any modes above 60 cm^{-1}, demonstrating that the alkali-type metal has little effect on the microstructure of the FeSe layer. Several additional modes appear below 60 cm^{-1} in Tl- and Rb-substituted samples, which are vibrations of heavier Tl and Rb ions. Finally, our calculations reveal the presence of "chiral" phonon modes, whose origin lies in the chiral nature of the $K_{0.8}Fe_{1.6}Se_2$ structure.

PACS numbers: 74.70.-b, 74.25.Kc, 63.20.kd, 78.30.-j

I. INTRODUCTION

Iron pnictide superconductors display the highest superconducting transition temperatures yet known outside cuprate systems. Unsurprisingly, their discovery almost four years ago ignited an enduring drive both to search for new superconducting materials and to explore the fundamental physical properties of these systems, especially the pairing mechanism. Until recently, five such systems had been synthesized and studied, namely LnFeAsOF (known as "1111," with Ln ≡ La, Ce, Pr, Nd, Sm, ...),[1] $AEFe_2As_2$ and AFe_2As_2 ("122," with AE an alkaline earth and A an alkali metal),[2] AFeAs ("111"),[3] Fe(Se,Te) ("11"),[4] and Sr_2VO_3FeAs ("21311").[5]

FeSe is of particular interest among these systems for a number of reasons. The most important is that it does not contain the poisonous element As. In addition, its transition temperature, T_c, displays a very strong pressure dependence. At ambient pressure, $T_c \approx 8$ K,[6] much lower than in the 1111 and 122 systems, but a maximum T_c of 37 K can be reached under a pressure of approximately 6 GPa.[7] It has been shown[6] that the microscopic effect of the applied pressure is to alter the separation of the Se atoms from the Fe planes, and this very strong dependence opens the possibility of raising T_c by the introduction of internal chemical pressure. The first successful execution of this program was reported in Ref. 8, where a potassium-intercalated FeSe superconductor was synthesized and found to have $T_c \approx 31$ K, a value comparable to that in the 122 materials.

In parallel with intensive efforts to synthesize further examples of $A_xFe_{2-y}Se_2$ systems, the electronic and magnetic properties of these compounds have been studied extensively. Infrared optical conductivity measurements indicated that the non-superconducting system is a small-gap semiconductor rather than a Mott insulator.[9] In superconducting samples, early nuclear magnetic resonance (NMR) measurements found very narrow line widths, singlet superconductivity with no coherence peak, and only weak spin fluctuations, but no sign of magnetism.[10] Angle-resolved photoemission spectroscopy (ARPES) measurements were initially inconclusive, but now[11] indicate three electron-like Fermi surfaces (two around the Γ point and one around the M point) with full gaps on at least two, but again no evidence for magnetic order. Both Raman[12] and infrared[9] spectroscopy find large numbers of phonon modes beyond those expected in a 122 structure, and transmission electron microscopy (TEM)[13] reveals a well-defined surface vacancy ordering.

The first piece of the puzzle concerning the true nature of the $A_xFe_{2-y}Se_2$ materials was revealed by neutron diffraction experiments.[14] First, these determine that the predominant structure is dictated by a real Fe content of 1.6 in the superconducting crystals. This gives a regular, 1/5-depleted Fe vacancy ordering pattern with a $\sqrt{5}\times\sqrt{5}$ unit cell. Second, the magnetic properties of this phase are perhaps the most unusual of any known superconductor, featuring an ordered spin structure of antiferromagnetically coupled four-spin blocks, a very high Néel temperature of 520 K, and an extraordinarily large local moment of $3.31\mu_B$ per Fe site.[14] The magnetic transition has now been confirmed by bulk measurements,[15] while Mössbauer spectroscopy has been used to verify the large local moment, giving results of 2.9 and $2.2\mu_B$ in two separate studies.[16] These observations demonstrate directly that the AFeSe superconductors are completely different from FeAs-based and cuprate superconductors in at least two respects. One is that a bulk ordering of the Fe vacancies plays a key role in determining the electronic and magnetic properties of the system. The other is the apparent (micro- or mesoscopic) coexistence of long-range antiferromagnetic order with superconductivity.

The question of coexistence is the other piece of the

puzzle. It involves reconciling the NMR and ARPES results, which appear to originate from a homogeneous, nonmagnetic bulk superconductor, with the data from all of the other techniques cited above, which are the signatures of a magnetic insulator with a complex structure. The nature of this coexistence or cohabitation has been the focus of almost all recent experimental investigations of the $A_xFe_{2-y}Se_2$ materials. A clear consensus has emerged in support of a phase separation between antiferromagnetic and superconducting regions, but occurring on microscopic length scales. Phase separation has been reported in optical[17] and ARPES experiments,[18] the former authors attributing a much larger direct band gap (0.45 eV) to the majority insulating phase than that deduced in Ref. 9. Very recent NMR measurements have detected clear signals from a majority magnetic phase as well as a minority superconducting one.[19] The appearance of phase separation occurring at nanometer scales has been detected by Mössbauer,[20] X-ray,[21] and in-plane optical spectroscopy measurements.[22] Scanning Tunneling Microscopy (STM) has been used to image this nanoscopic phase separation directly in epitaxially grown films.[23] Estimates of the volume fraction of the magnetic and insulating phase by these techniques remain close to the value of 90% reported by muon spin resonance (μSR) measurements.[24] The minority (10%) superconducting phase must clearly be percolating to give the appearance of bulk superconductivity. Several studies[18,19,23,25] indicate that the ordered vacancy configuration is present only in the AF phase, consistent with the unusual magnetism being an essential component in stabilizing this structure, while the superconducting phase is structurally homogeneous with stoichiometric FeSe planes (some authors[18,23,25] suggesting AFe_2Se_2). Finally, there are only two experimental reports concerning the question of whether this coexistence is collaborative or competitive; our own data from two-magnon Raman scattering[26] and additional results from neutron diffraction[27] suggest a strong competition, in that $5-10\%$ of the magnetic volume is suppressed by an apparent proximity effect at the onset of superconductivity.

Returning to the question of sample synthesis, rapid progress followed the first report of $K_xFe_{2-y}Se_2$, with several groups achieving superconductivity by substitution of alkali-type metals including Rb, Cs, and Tl.[28] The purpose of substitution by ions of equal valence but different radii is to alter the chemical pressure to control the electronic properties. An example is the maximum T_c of approximately 56 K achieved by the substitution of rare-earth ions in the 1111 system.[29] It is thus somewhat surprising that substitution of K by Rb, Cs, or Tl in the new superconductors leaves T_c essentially unaltered at around 30 K.[28] This result poses another fundamental question, concerning why superconductivity should be so robust in the AFeSe system, and its answer requires a careful investigation into the effect of Tl, Rb, and Cs substitution on the microstructure of the FeSe layers in these materials.

In this paper, we address these questions through a Raman-scattering study. We have measured the spectra in three high-quality superconducting crystals of Tl- and Rb-substituted $K_{0.8}Fe_{1.6}Se_2$, and in one non-superconducting crystal with an altered Fe content. For each crystal, we observe double-digit numbers of phonon modes, dramatically different from a normal 122 structure but consistent with an ordered vacancy structure. We perform first-principles calculations for the zone-center phonons in $K_{0.8}Fe_{1.6}Se_2$ (T_c = 32 K), in order to assign the observed modes by the symmetries and frequencies we measure. The resulting assignment is very satisfactory, demonstrating that this vacancy-ordered structure is indeed the majority phase of our samples. From this understanding, we find the effect of a varying Fe content to be detectable as frequency shifts of the Raman modes above 60 cm^{-1}, as these are vibrations involving Fe and Se atoms. By contrast, the effects of Tl and Rb substitution are not discernible above 60 cm^{-1}, indicating that K-layer substitution causes no substantial distortion of the FeSe layer. Below 60 cm^{-1}, additional modes associated with vibrations of the heavier Tl and Rb ions can be observed in the substituted samples. In our calculations we also find some unconventional "chiral" phonon modes, which arise due to the chiral nature of the $\sqrt{5} \times \sqrt{5}$ Fe-vacancy structure, and we consider their implications for coupling to possible chiral electronic and magnetic modes.

The structure of the manuscript is as follows. In Sec. II we discuss our sample preparation and measurement techniques. In Sec. III we present the full theoretical analysis for computing the phonon spectrum from the known lattice structure of the insulating and magnetic majority phase, and we discuss the nature of the predicted modes. With this frame of reference, we may then understand our Raman-scattering results, which are presented in detail in Sec. IV. Section V contains a short summary and conclusion.

II. MATERIALS AND METHODS

The FeSe-based crystals used in our measurements were grown by the Bridgman method. The detailed growth procedure may be found elsewhere.[30] The accurate determination of crystal stoichiometry has been found to be a delicate issue, which is crucial in establishing the proper starting point for understanding both the magnetism and the superconductivity. We have obtained highly accurate results for our crystal compositions by using inductively coupled plasma atomic emission spectroscopy (ICP-AES), and have obtained results completely consistent with the neutron diffraction refinement.[14] The crystals we used in this study were $K_{0.8}Fe_{1.6}Se_2$ ($T_c \approx 32$ K), $Tl_{0.5}K_{0.3}Fe_{1.6}Se_2$ ($T_c \approx 29$ K), and $Tl_{0.5}Rb_{0.3}Fe_{1.6}Se_2$ ($T_c \approx 31$ K), all of which were superconducting with similar transition temperatures, and also the non-superconducting compound $KFe_{1.5}Se_2$. The

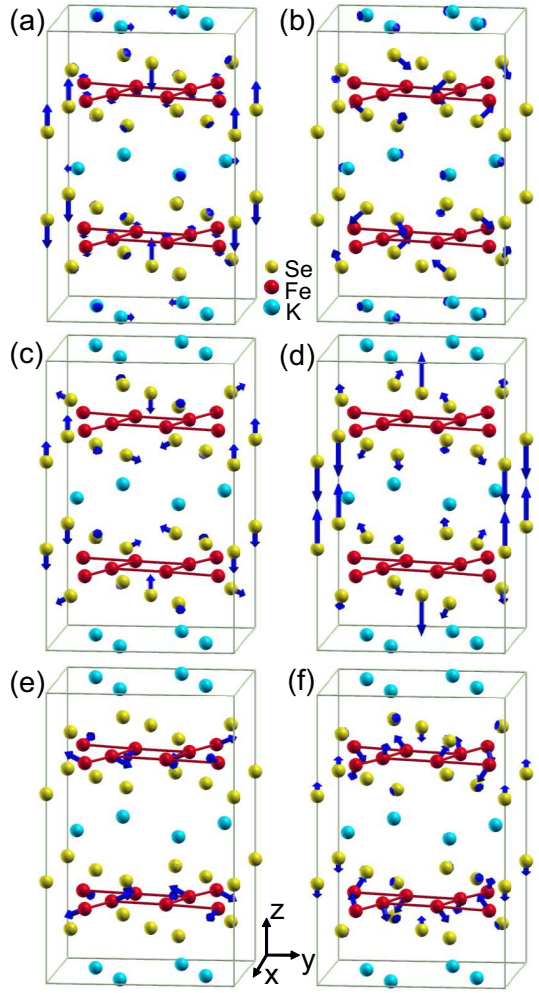

FIG. 1: (Color online) Atomic displacement patterns for selected Raman-active A_g modes of $K_{0.8}Fe_{1.6}Se_2$, with frequencies of (a) 75.1, (b) 130.5, (c) 159.2, (d) 212.6, (e) 268.5, and (f) 286.1 cm^{-1}. Fe atoms connected by red lines have right-handed chirality in this representation.

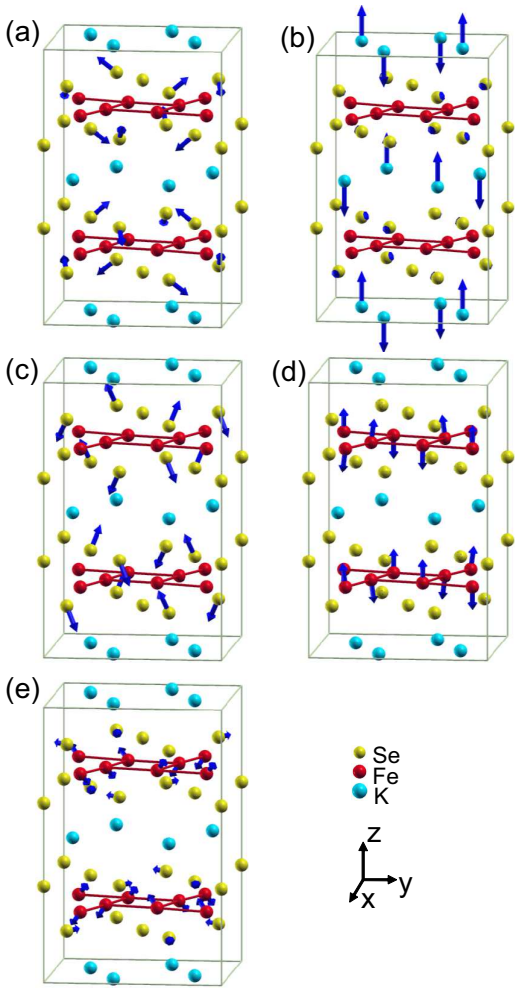

FIG. 2: (Color online) Atomic displacement patterns for selected Raman-active B_g modes of $K_{0.8}Fe_{1.6}Se_2$ with frequencies of (a) 66.7, (b) 106.2, (c) 149.0, (d) 238.3, and (e) 279.0 cm^{-1}. Fe atoms connected by red lines have right-handed chirality.

precise chemical formula for this series of compounds is thought to be $A_xFe_{2-x/2}Se_2$ (A = K, Rb, Cs, Tl),[14,31] and our results agree with this deduction. The above discussion of phase separation notwithstanding, X-ray diffraction patterns obtained for our crystals show no discernible secondary phases, indicating that the volume fraction of the superconducting minority phase is low in all cases. The resistivities of the samples were measured with a Quantum Design physical properties measurement system (PPMS), and the magnetization by using the PPMS vibrating sample magnetometer (VSM). The sharp superconducting and diamagnetic transitions, which were found for all three superconducting crystals, are presented in Sec. IV to accompany a more detailed discussion of phase separation. These results indicate that all of the crystals used in our Raman measurements are of very high quality, which in a phase-separation context means that the nanoscale percolation of the minority phase is good and homogeneous.

All measurements were made by first cleaving the crystals in a glove box, to obtain flat, shiny (ab)-plane surfaces. The freshly-cleaved crystals were sealed under an argon atmosphere and transferred into the cryostat within 30 seconds for immediate evacuation to a work vacuum of approximately 10^{-8} mbar. Raman-scattering measurements were performed with a triple-grating monochromator (Jobin Yvon T64000) in a pseudo-backscattering configuration. The beam of the 532 nm solid-state laser (Torus 532, Laser Quantum) was focused into a spot on the sample surface with a diameter of approximately 20 μm. The beam power was reduced to avoid heating, and was kept below 0.6 mW during our measurements at the lowest temperatures; the real temperature in the spot was deduced from the intensity relation between the Stokes and anti-Stokes spectra. The polarization determination for the phonons whose sym-

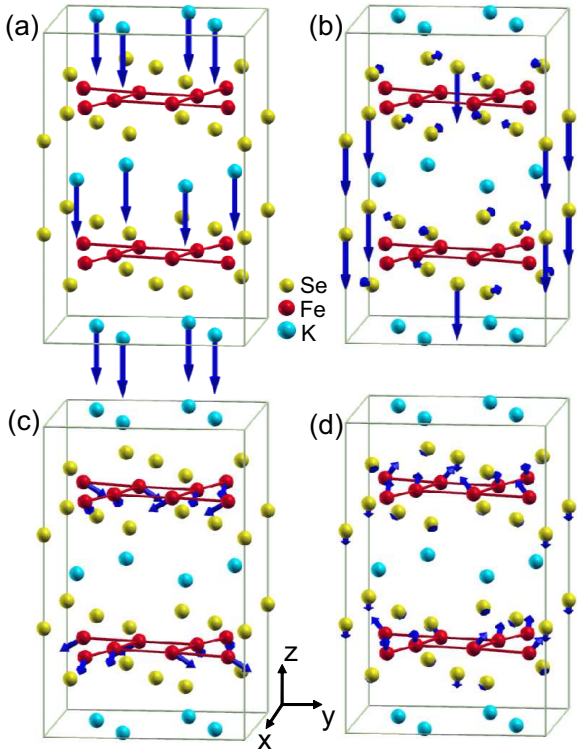

FIG. 3: (Color online) Atomic displacement patterns for selected infrared-active phonon modes of $K_{0.8}Fe_{1.6}Se_2$ with frequencies of (a) 119.1, (b) 212.3, (c) 253.4, and (d) 308.5 cm^{-1}. Fe atoms connected by red lines have right-handed chirality.

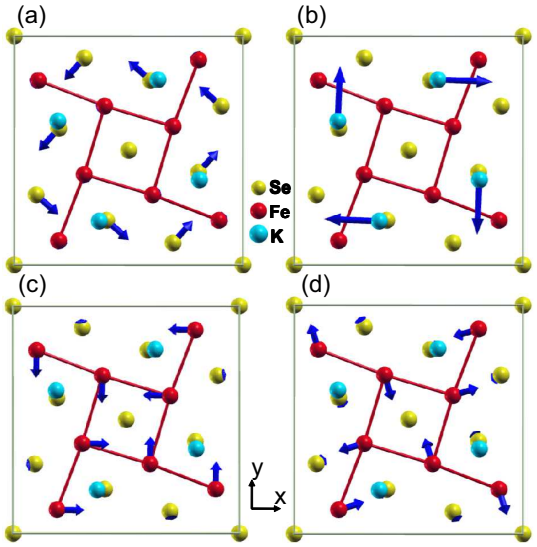

FIG. 4: (Color online) Atomic displacement patterns for chiral phonon modes [(a) 67.0, (b) 86.2, and (c) 301.3 cm^{-1}] and for the breathing mode [(d) 269.6 cm^{-1}] of $K_{0.8}Fe_{1.6}Se_2$. Fe atoms connected by red lines have right-handed chirality.

metries we assign as A_g and B_g in the spectra shown in Sec. IV was performed by adjusting the polarization of the incident and scattered light, rather than by a formal symmetry analysis, as discussed in detail in Ref. 12.

III. FIRST-PRINCIPLES DYNAMICAL ANALYSIS

A full understanding of our Raman-scattering results, and in particular of the effects caused by iron content and potassium substitution, requires a complete phonon mode assignment. The ordered pattern of Fe vacancies[14] explains quite naturally the large number of optical phonons observed in light-scattering experiments. However, the large unit cell means that a detailed vibration analysis is somewhat involved. We begin with the results from neutron diffraction,[14] which gives the structural space group of $K_{0.8}Fe_{1.6}Se_2$ as $I4/m$ and the Wyckoff positions of the atoms as 8h for potassium, 16i for iron, 4d for the iron vacancies, and 16i for selenium. The corresponding symmetry analysis allows a total of 17 A_g or B_g modes.[12]

We have calculated the nonmagnetic electronic structure and the zone-center phonons of $K_{0.8}Fe_{1.6}Se_2$ from first principles by performing density-functional calculations. We use the Vienna *ab-initio* simulation package,[32,33] which makes use of the projector augmented wave (PAW) method[33] combined with a general gradient approximation (GGA), implemented with the Perdew-Burke-Ernzerhof formula,[34] for the exchange-correlation potentials. The nonmagnetic $K_{0.8}Fe_{1.6}Se_2$ system was modeled by adopting a parallelepiped supercell containing 8 Fe atoms plus 2 Fe vacancies, 10 Se atoms, and 4 K atoms plus 1 K vacancy. The Brillouin zone of the supercell was sampled with an $8\times8\times8$ **k**-space mesh and the broadening was taken to be Gaussian. The energy cutoff for the plane waves was 400 eV. Both the shape and volume of the cell and the internal coordinates of all the ions were fully optimized until the forces on all relaxed atoms were below 0.01 eV/Å.

The frequencies and displacement patterns of the phonon modes were calculated using the dynamical matrix method,[35] in which the derivatives were taken from the finite differences in atomic forces at a fixed atomic displacement of 0.01 Å. All 22 atoms in the supercell were allowed to move from their equilibrium positions in all directions (x, y, z), leading to a 66×66 matrix. The phonon frequencies and displacement patterns are given by diagonalizing this matrix. Convergence tests carried out by comparing the different **k**-points assured that the final results were well converged both in their overall energetics and in the phonon spectrum (yielding accuracies of order 2 cm^{-1}). The 22-atom supercell has 63 optical modes. However, to illustrate the displacement patterns of the phonon modes deduced from real-space translational invariance, in Figs. 1–3 we show our results in the 44-atom $I4/m$ cell.

Calculated phonon frequencies for prominent modes of all symmetries are listed in Table I. The experimental

TABLE I: Symmetry analysis for space group $I4/m$ and assignment of selected optical modes in $K_{0.8}Fe_{1.6}Se_2$. The "=", "$\perp$", and "$\angle$" symbols denote respectively eigenmode directions parallel, perpendicular, and at an angle to the FeSe plane of the crystal.

Atom	Wyckoff position	Optical modes	
		Raman active	Infrared active
K	8h	$2A_g + 2B_g + 2E_g$	$A_u + 4E_u$
Fe	16i	$3A_g + 3B_g + 6E_g$	$3A_u + 6E_u$
Se	4e	$A_g + 2E_g$	$A_u + 2E_u$
Se	16i	$3A_g + 3B_g + 6E_g$	$3A_u + 6E_u$

Cal. Freq. (cm^{-1})	Expt. Freq. (cm^{-1})	Symmetry	Index	Atoms	Direction of eigenmode			
					K(8h)	Fe(16i)	Se(4e)	Se(16i)
66.7	61.4	B_g	^1B_g	Se				$\angle$
75.1	66.3	A_g	^1A_g	Se			$\perp$	
106.2	100.6	B_g	^2B_g	K	$\perp$			
130.5	123.8	A_g	^2A_g	Se				$\angle$
159.2	134.6	A_g	^3A_g	Se			$\perp$	$\angle$
149.0	141.7	B_g	^3B_g	Se				$\angle$
212.6	202.9	A_g	^4A_g	Se			$\perp$	$\angle$
238.3	214.3	B_g	^4B_g	Fe		$\perp$		
268.5	239.4	A_g	^5A_g	Fe		$\angle$		
286.1	264.6	A_g	^6A_g	Fe,Se		$\angle$	$\perp$	
279.0	274.9	B_g	^5B_g	Fe		$\angle$		
83.3		E_g		K,Se	$\perp$			$\angle$
102.4		E_g		K,Se	$\perp$		=	=
143.4		E_g		Se			=	=
208.7		E_g		Se			=	$\angle$
242.5		E_g		Fe,Se		$\angle$	=	
284.9		E_g		Fe,Se		$\angle$	=	
119.1	102.2[a]	A_u		K	$\perp$			
212.3	208.3[a]	A_u		Se			$\perp$	$\angle$
253.4	236.3[a]	A_u		Fe		$\angle$		
308.5		A_u		Fe,Se		$\angle$	$\perp$	
67.0		Chiral		Se				$\angle$
86.2		Chiral		K	=			
301.3		Chiral		Fe		=		
269.6		Breathing		Fe		$\angle$		

[a]Ref. 36.

frequencies are discussed in Sec. IV. As expected, the majority of the modes are vibrations related to the Fe and Se atoms in the primary structural unit, and this includes all but one of the experimentally relevant modes (Table I). Vibrations of the K atoms appear only at low energies, reflecting the weak restoring forces they encounter far from the FeSe planes. In the real material, these atoms are thought to be rather mobile.

The atomic displacement patterns of the assigned A_g and B_g modes are shown respectively in Figs. 1 and 2. The displacement arrows are to scale between panels, and it is clear that the largest atomic motions are in the c-direction, while in-plane motion is more restricted. The right-hand columns of Table I detail the character of the calculated eigenmodes, showing whether they correspond to atomic motions primarily in the FeSe plane, perpendicular to it, or in a genuine combination of both. In addition to the dominant A_g and B_g modes, we also compute a number of E_g phonons over the same frequency range and list some selected modes in Table I; these two-fold degenerate modes correspond to in-plane atomic motions, although they may obtain weak normal components due to the presence of the vacancies. For reasons of light-scattering selection rules, these modes are not usually observed in Raman experiments for approximately tetragonal materials.

The optical phonons we have calculated include not only the Raman-active modes but also similar numbers of infrared-active ones. Four selected examples are also listed in Table I and compared to recent experimental measurements, while their displacement patterns are illustrated in Fig. 3. As for the Raman-active modes, most of the infrared modes are vibrations of the Fe and Se atoms. In the tetragonal 122 iron arsenide superconductors, there exist just two ideal, one-dimensional Raman-active phonon modes of the FeAs plane, whose

TABLE II: Eigenvectors of the most important atoms involved in selected vibrational modes of $K_{0.8}Fe_{1.6}Se_2$ (Table I). Directions x, y, and z are those shown in Figs. 1−4.

Cal. Freq.	Symmetry	Eigenvector (x y z)			
(cm^{-1})		K(8h)	Fe(16i)	Se(4e)	Se(16i)
66.7	B_g				(-0.07 0.24 0.20)
75.1	A_g			(0.00 0.00 0.34)	
106.2	B_g	(0.00 0.00 0.39)			
130.5	A_g				(0.20 0.12 0.20)
159.2	A_g			(0.00 0.00 0.29)	(-0.07 0.22 0.11)
149.0	B_g				(0.11 0.13 0.29)
212.6	A_g			(0.00 0.00 0.40)	(-0.04 0.11 0.23)
238.3	B_g		(0.00 0.04 0.31)		
268.5	A_g		(0.10 0.27 0.12)		
286.1	A_g		(0.15 0.08 0.23)	(0.00 0.00 0.24)	
279.0	B_g		(-0.15 0.12 0.19)		
83.3	E_g	(0.00 0.00 0.17)			(0.12 0.14 0.05)
102.4	E_g	(0.00 0.00 0.28)		(-0.12 0.22 0.00)	(-0.03 0.24 0.01)
143.4	E_g			(-0.25 0.18 0.00)	(-0.11 0.29 0.04)
208.7	E_g			(0.34 -0.04 0.00)	(0.24 -0.04 0.15)
242.5	E_g		(0.19 -0.03 0.22)	(-0.06 0.26 0.00)	
284.9	E_g		(0.24 -0.02 0.07)	(-0.19 0.18 0.00)	
119.1	A_u	(0.00 0.00 -0.46)			
212.3	A_u			(0.00 0.00 -0.45)	(0.13 0.22 0.08)
253.4	A_u		(0.03 0.27 -0.16)		
308.5	A_u		(0.01 0.17 0.22)	(0.00 0.00 -0.23)	
67.0	Chiral				(0.20 0.23 0.06)
86.2	Chiral	(0.02 0.42 0.00)			
301.3	Chiral		(0.01 0.29 0.00)		
269.6	Breathing		(-0.08 0.27 0.09)		

symmetries are A_{1g} and B_{1g},[37] and similarly just two infrared-active modes. To the extent that $K_{0.8}Fe_{1.6}Se_2$ can be considered as an ordered, 1/5-depleted version of this system, it is clear that the symmetry reduction and expansion of the unit cell allow many more Raman- and infrared-active optical modes to exist in the alkali-intercalated FeSe superconductors.

Table II contains the full details of the eigenvectors for the atomic displacements corresponding to all of our selected modes. While much more specialized than the polarization information, we provide this data for completeness and specificity concerning the representations in Figs. 1−4. A full understanding of experimental data concerning resistivity, pairing, and anomalies in ARPES, inelastic neutron scattering, and magnetic Raman signals depends on an accurate knowledge of the phonon spectrum, and the quantitative intensity (Sec. IV) and polarization information we provide can be used to calculate the interactions between specific phonon modes and the itinerant electrons or spin fluctuations of the charge and spin sectors.

As an immediate example of this, in our calculations we also find some novel "chiral" phonon modes, whose atomic displacement patterns are shown in Fig. 4. These are nondegenerate and primarily in-plane modes in which all the Fe or Se atoms in a single plane of the structural unit have a net rotation about the center of the cell, an apparent angular momentum canceled by the atomic displacements in neighboring unit cells of the same FeSe layer. The presence of these chiral modes is a direct consequence of chiral symmetry-breaking in the AFeSe system when the 1/5-depleted vacancy structure is adopted; the $\sqrt{5} \times \sqrt{5}$ unit cell[14] itself has an explicit left- or right-handed structural chirality.[38] The chiral phonon modes are not active in the Raman channel, and therefore are not observed in the Raman measurements performed here. We suggest, however, that these chiral modes may be observed by different spectroscopic techniques in circular polarization configurations.

The presence of chiral modes is of particular interest as a possible probe of chiral electronic or magnetic excitations, which break time-reversal symmetry. Such excitations have been discussed in the parent compounds of cuprate superconductors, where an A_2 component attributed to chiral spin excitations was detected by Raman scattering.[39] At the theoretical level, a chiral d-density-wave state has also been proposed in the underdoped state of cuprate superconductors.[40] Such modes, involving chiral electronic motion, may couple preferentially to the chiral phonon vibration in the 1/5-depleted AFeSe system, in the same way as phonons of B_{1g} symmetry couple to the d-wave superconducting order parameter in cuprates, and thus Raman phonon spectroscopy may be used to detect their presence. Without such a cou-

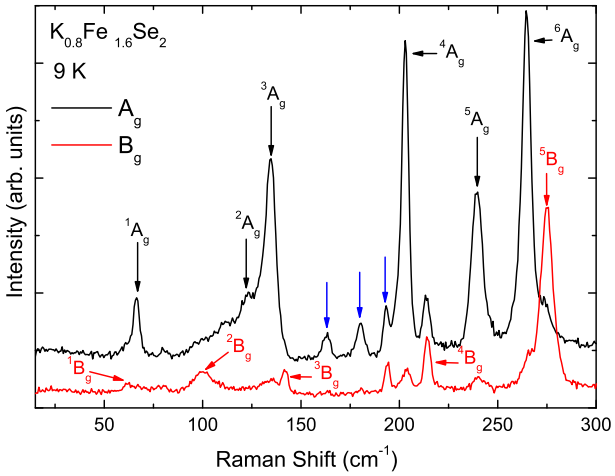

FIG. 5: (Color online) Raman spectra for $K_{0.8}Fe_{1.6}Se_2$, measured in the A_g and B_g channels at 9 K. The mode assignment is made on the basis of the symmetry analysis and the first-principles calculations of Sec. III. The corresponding atomic displacement patterns can be found in Figs. 1 and 2. Blue arrows indicate unassigned modes.

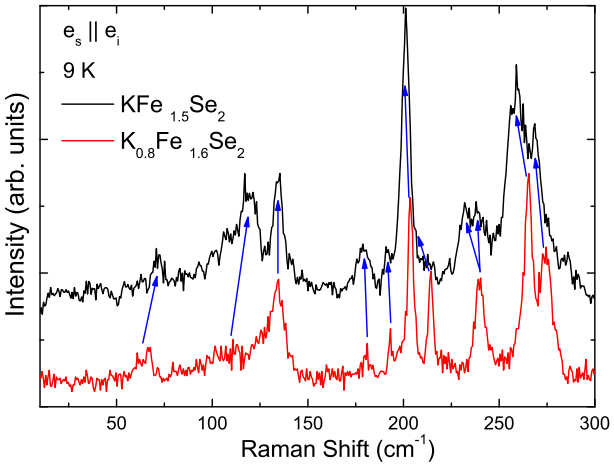

FIG. 6: (Color online) Comparison between Raman spectra of $K_{0.8}Fe_{1.6}Se_2$ and $KFe_{1.5}Se_2$. Labels e_i and e_s denote respectively the polarizations of the incident and scattered light.

pling to phonon modes, any chiral electronic or magnetic excitations in the AFeSe system may also be subject to direct detection by the polarized spectroscopies, such as ARPES and neutron scattering, also applied in the study of cuprates.

IV. RAMAN-SCATTERING MEASUREMENTS

We begin the presentation of our Raman-scattering results by recalling the basic features the low-temperature spectra, which are shown for $K_{0.8}Fe_{1.6}Se_2$ in Fig. 5. The measurements were performed at 9 K in polarization configurations which separate the A_g and B_g channels. At least thirteen Raman-active modes are observed, all located below 300 cm^{-1};[12] at least ten infrared-active modes have also been measured[9] in the same frequency range. This abundance of optical modes arises due to the symmetry reduction caused by Fe vacancy ordering, which we have identified as being from D_{4h} to C_{4h}.[12] The space group of the undepleted, 122-type structure, $I4/mmm$, is reduced to $I4/m$, a process in which all in-plane, two-fold rotation axes and all mirror planes perpendicular to the (ab)-plane are lost. Both the phonon mode energies and the polarizations observed in Fig. 5 are in excellent agreement with the calculations of Sec. III for the spectrum of optical modes (Table I), as also are the measured infrared modes.[36]

A. Fe content

In Fig. 6 we compare the Raman modes in superconducting $K_{0.8}Fe_{1.6}Se_2$ with those in non-superconducting $KFe_{1.5}Se_2$. The modes in the two samples show a general similarity in intensity and location, which implies a similarity in the microstructures and symmetries of their FeSe layers. However, it is also evident that changing the Fe content does cause a significant shift in frequency for most of the modes. Because these modes are vibrations involving the Fe and Se ions (Tables I and II), this reflects some significant differences between the FeSe layers in the two samples. As noted above, neutron diffraction measurements confirm that the majority phase of the system at an Fe stoichiometry of 1.6 (20% Fe vacancies) forms the ideal, four-fold-symmetric, 1/5-depleted, $\sqrt{5}\times\sqrt{5}$ vacancy-ordering pattern. These measurements also indicate[14] that the same ordering pattern is maintained for the sample with an Fe content of 1.5, despite the increase to 25% Fe vacancies; in this case the 16i Fe positions are only partially occupied. This occupation means a random distortion of the Fe-Se bonds, which is responsible for the shifts in mode frequencies. Our results are thus in agreement with those from neutron diffraction, confirming that the electronic and magnetic properties of the AFeSe system are rather sensitive to the vacancy content of the FeSe layers, even if the overall layer structure is not. These changes should thus be considered as disorder effects rather than microstructural effects. Altering the Fe content from 1.6 to 1.5 causes our sample to become an insulator with a small gap, which is estimated by infrared experiments to be 30 meV,[9] and by transport measurements to be approximately 80 meV.[31]

B. K substitution

Raman spectra for the three superconducting crystals $K_{0.8}Fe_{1.6}Se_2$, $Tl_{0.5}K_{0.3}Fe_{1.6}Se_2$, and $Tl_{0.5}Rb_{0.3}Fe_{1.6}Se_2$ are shown in Fig. 7. In contrast to the case of changing Fe content discussed above, the modes above 60 cm^{-1}

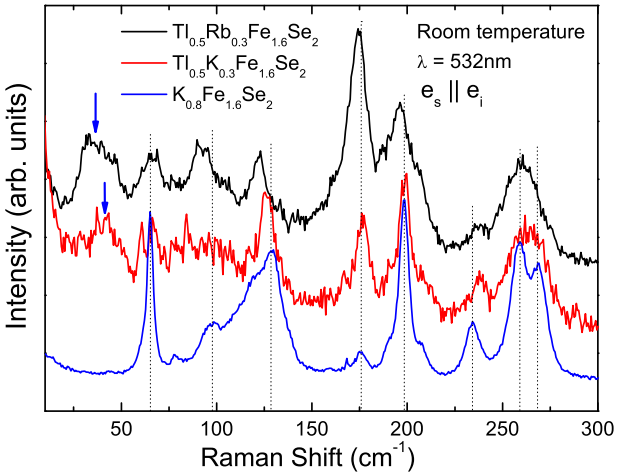

FIG. 7: (Color online) Raman spectra of the three superconducting crystals at room temperature. Additional modes, indicated by blue arrows, appear below 60 cm^{-1} in the Tl- and Rb-substituted samples. Dotted lines are guides indicating the peak positions.

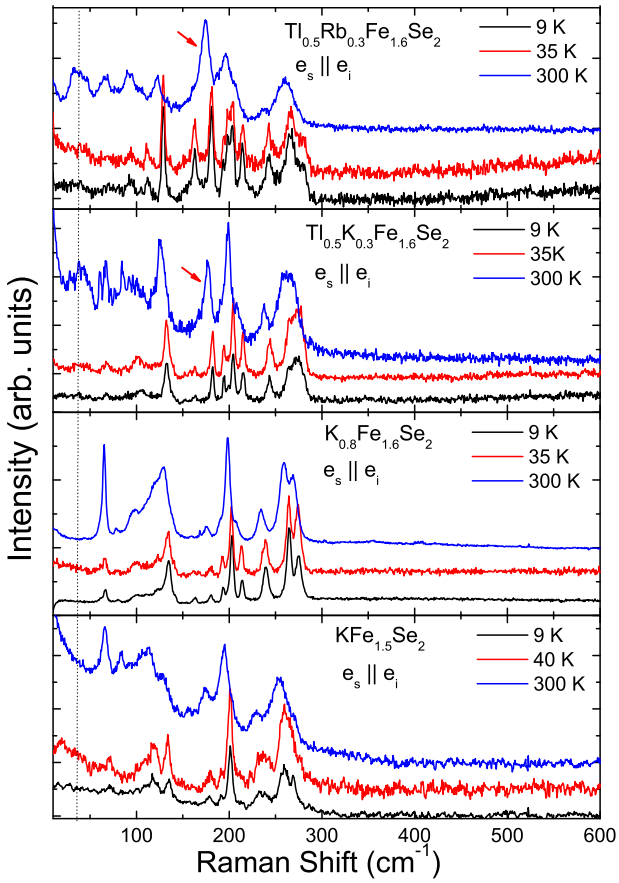

FIG. 8: (Color online) Raman spectra of superconducting and non-superconducting AFeSe systems at selected temperatures. The dotted line indicates the location of additional modes induced by K substitution and the red arrows indicate modes showing large changes of intensity between different crystals.

exhibit no substantial shift in frequency (although there are clear differences in relative intensities). This suggests that substitution within the potassium layers (at fixed Fe content) has little effect on the FeSe layer, and essentially none on the ordering pattern of the Fe vacancies. This substitution does, however, cause certain other changes to occur. The most notable is the presence of some additional phonon modes, which appear below 60 cm^{-1}. These modes can be attributed unambiguously to vibrations of the heavier Tl and Rb ions, which are absent in the spectra of $K_{0.8}Fe_{1.6}Se_2$ (Figs. 5 and 6) and $KFe_{1.5}Se_2$ (Figs. 6 and 8). The other important alteration is the dramatic intensity enhancement of the mode at 180 cm^{-1}, which has A_g character but cannot (Fig. 5) be assigned well from the calculations of Sec. III; we discuss this feature in detail below.

The additional low-frequency modes induced by K-substitution are shown in Fig. 8. These become weaker but not narrower with decreasing temperature, eventually disappearing at 9 K. This behavior is similar to that of the 66 cm^{-1} Se A_g mode, which largely follows the Bose-Einstein thermal factor.[12] By comparison with $K_{0.8}Fe_{1.6}Se_2$, these modes may readily be identified as vibrations of heavier Tl and Rb ions. It should also be noted here that there exist two possible Wyckoff positions for the A ions, namely 2a and 8h, and that no Raman-active modes are allowed for atoms in the 2a positions. No structural transition is found below the Néel temperature (520 K) in neutron-diffraction studies of $K_{0.8}Fe_{1.6}Se_2$,[14] and the temperature-dependent Raman spectra in Fig. 8 show that it is reasonable to assume the same behavior in the Tl- and Rb-substituted crystals. We therefore deduce that the additional modes are allowed due to changes of the local symmetry in the (Tl,K/Rb)-layer, for which a random occupation of 2a and 8h sites by A ions is the most likely possibility.

C. Discussion

We begin our discussion with the anomalous 180 cm^{-1} mode. This shows not only a curious temperature-dependence of its intensity between samples, but also of its frequency at T_c. The fact that this mode cannot be assigned properly by our symmetry analysis and first-principles calculations suggests that it may be a local mode. One of the most likely candidates for this would be a nanoscopic region where the Fe vacancy is filled, creating a locally regular square lattice. Indeed, the As A_{1g} mode in the 122 compounds occurs at a frequency of 182 cm^{-1} in $SrFe_2As_2$.[37]

A locally regular square lattice is also one of the leading candidates suggested in the phase-separation description of the FeSe superconductors. As noted in Sec. I, several authors have proposed that the superconducting minority phase is AFe_2Se_2,[18,23,25] while others[19] agree with the

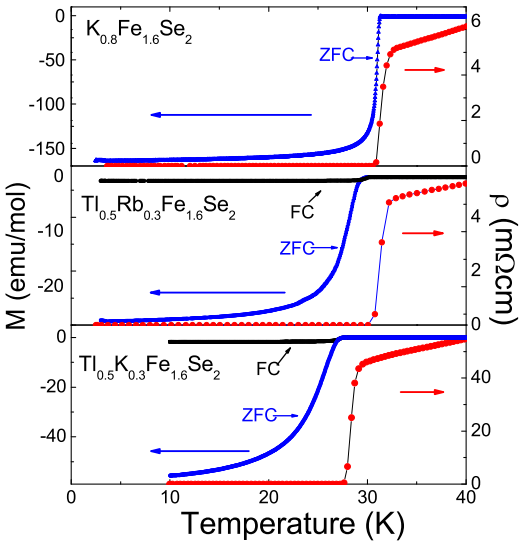

FIG. 9: (Color online) Superconducting and diamagnetic transitions for the three superconducting crystals used in the Raman-scattering investigations.

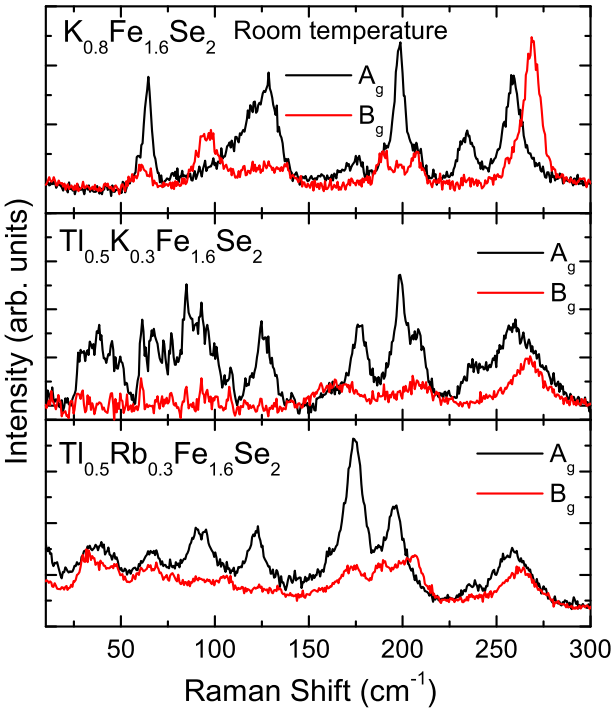

FIG. 10: (Color online) Polarized Raman spectra of the three superconducting crystals, showing that phonon widths are generally lower in $K_{0.8}Fe_{1.6}Se_2$.

stoichiometric FeSe planes but not with the A content. This scenario, that the 180 cm^{-1} mode we observe is not merely a local filled vacancy, but the leading fingerprint of a 122-like ($A_xFe_2Se_2$) minority phase, would also be consistent with the jump we observe in the frequency of this mode at T_c, which suggests a strong coupling of this specific mode to the superconducting order parameter. Further evidence in favor of this interpretation could be found in the B_{1g} mode of the 122-type structure, which appears at 204 cm^{-1} in $SrFe_2As_2$.[37] Our results do contain a B_g component very close to this frequency, but we caution that it is accompanied by a very strong A_g signal, and may only be a shadow of this mode arising due to a disorder-induced mixing of local symmetries.[41]

In the general context of phase separation, it is clear that our samples have both a robust structural and magnetic order (from the neutron diffraction studies performed on the same crystals) and a clear superconducting component. We have been unable to find any evidence for the presence of secondary phases in X-ray and neutron-scattering studies,[14,42] and we show in Fig. 9 that the resistive and diamagnetic transitions at the onset of superconductivity are sharp and continuous in all three samples. However, as pointed out by many authors, none of these results is sufficient to exclude minority phases with a low volume fraction, and the data for the superconducting transitions show only that the percolation of the superconducting fraction is complete and homogeneous (which would be consistent with a microscale phenomenon).

In the most extreme version of a phase-separation scenario, only the 122-like ($A_xFe_2Se_2$) and 245 ($A_{0.8}Fe_{1.6}Se_2$) phases would exist, and altering Fe content would affect only their ratio. While this situation would account for a loss of superconductivity on reducing the Fe content, it does seem to require at least one further low-Fe phase in the doping range of our samples. Our results do not support this scenario. It would predict that changes in the Fe stoichiometry in Fig. 6 should appear only as alterations in phonon intensity, rather than to the phonon frequencies as we observe. Our results definitely indicate continuous alterations to a single majority phase, and show further that some vacancy-disorder effects are clearly (if not strongly) detectable. Thus we conclude that our Raman phonon spectra contain no unambiguous evidence for a robust, 122-like minority phase, and we suggest rather a phase-separation scenario in which the minority phase is one of homogeneous vacancy disorder.

Returning now to the anomalous phonon modes, both scenarios (a secondary 122-like phase and locally filled Fe vacancy sites) can account qualitatively for the frequencies of additional phonon modes beyond our dynamical analysis. While both also explain the anomalous behavior of the 180 cm^{-1} mode at T_c, neither accounts directly for the anomalous intensity of this mode. To explain this, we note that the assignment of the mode as a (local or bulk) version of the 122 A_{1g} mode means that it involves a c-axis displacement of the Se atoms. These are the FeSe modes most strongly affected (Figs. 7 and 8) by A-induced changes in the local microstructure, and we suggest that these alter the mode intensity in the same way as for the 66 cm^{-1} mode.[12]

Away from the nature of the phase separation, we com-

ment also on the distinctive low-energy background observed for the four crystals we have measured (Fig. 8). The spectrum of semiconducting $KFe_{1.5}Se_2$ at room temperature rises strongly at low frequencies, whereas the low-energy part for $K_{0.8}Fe_{1.6}Se_2$ is rather flat. All of the background contributions fall with decreasing temperature. We suggest that the low-frequency enhancement may be due to electronic Raman scattering. Because $KFe_{1.5}Se_2$ is a small-gap semiconductor, the smaller Coulomb screening effect relative to a normal metal would allow stronger charge-density fluctuations and hence a larger electronic Raman scattering contribution.

Finally, one of the most surprising features of the $K_{0.8}Fe_{1.6}Se_2$ material that makes up the majority of our samples is its apparently high degree of structural order. This occurs despite its depleted nature, which one would expect to be prone to atomic disorder. Evidence for disorder can in fact be found in the polarized Raman spectra at room temperature (Fig. 10). The Tl- and Rb-substituted samples show larger phonon widths compared to $K_{0.8}Fe_{1.6}Se_2$, which implies that more disorder is induced by the substitution. Given that no substantial shifts occur in the mode frequencies for the three samples, this disorder can be attributed to the random occupation and motion of the K, Tl, and Rb ions. The breaking of local symmetry and periodicity in the A layer acts to shorten the phonon lifetimes also in the FeSe layer. Overall, it appears that the high stability of the $\sqrt{5} \times \sqrt{5}$ vacancy-ordered structure, which assures the constant frequencies of the phonon modes we observe in all our superconducting samples, may be a consequence of the very specific magnetically ordered state it allows.

V. SUMMARY

To conclude, we have measured Raman spectra in single-crystalline samples of the superconductors $K_{0.8}Fe_{1.6}Se_2$, $Tl_{0.5}K_{0.3}Fe_{1.6}Se_2$, and $Tl_{0.5}Rb_{0.3}Fe_{1.6}Se_2$, as well as in their insulating derivative compound $KFe_{1.5}Se_2$. A symmetry analysis and first-principles calculations of the zone-center phonons, both based on the $\sqrt{5} \times \sqrt{5}$ vacancy-ordering pattern of the $K_{0.8}Fe_{1.6}Se_2$ unit cell, allow an excellent assignment of the observed phonon modes. We illustrate the corresponding atomic displacement patterns and demonstrate the presence of chiral phonon modes.

We observe a clear frequency shift in all phonons between superconducting $K_{0.8}Fe_{1.6}Se_2$ and non-superconducting $KFe_{1.5}Se_2$, showing the effect of further Fe vacancies within the $\sqrt{5} \times \sqrt{5}$ structure on the microscopic properties of the FeSe layers. By contrast, the frequencies of modes involving Fe and Se ions are little affected on substituting K by Tl or Rb. However, this substitution does induce additional Tl and Rb modes below 60 cm^{-1}. Our measurements also contain a number of anomalies, which may be purely effects of the intrinsic vacancy disorder or may be explained in part by the presence of the weak minority phase responsible for superconductivity. Our results reveal the complex effects of Fe vacancies in the FeSe plane, laying the foundation for a full understanding of the distinctive structural, electronic, magnetic, and superconducting properties of the $A_xFe_{2-y}Se_2$ series of materials.

Acknowledgments

We thank W. Bao and Z. Y. Lu for helpful discussions. This work was supported by the 973 program of the MoST of China under Grant Nos. 2011CBA00112&2012CB921701, by the NSF of China under Grant Nos. 11034012, 11174367 and 11004243, by the Fundamental Research Funds for Central Universities, and by the Research Funds of Renmin University of China (RUC). Computational facilities were provided by the HPC Laboratory in the Department of Physics at RUC. The atomic structures and displacement patterns were plotted using the program XCRYSDEN.[43]

* Electronic address: qmzhang@ruc.edu.cn

[1] Y. Kamihara, H. Hiramatsu, M. Hirano, R. Kawamura, H. Yanagi, T. Kamiya, and H. Hosono, J. Am. Chem. Soc. **128**, 10012 (2006); X. H. Chen, T. Wu, G. Wu, R. H. Liu, H. Chen, and D. F. Fang, Nature **453**, 761 (2008); G. F. Chen, Z. Li, D. Wu, G. Li, W. Z. Hu, J. Dong, P. Zheng, J. L. Luo, and N. L. Wang, Phys. Rev. Lett. **100**, 247002 (2008).

[2] M. Rotter, M. Tegel, and D. Johrendt, Phys. Rev. Lett. **101**, 107007 (2008).

[3] X. C. Wang, Q. Q. Liu, Y. X. Lv, W. B. Gao, L. X. Yang, R. C. Yu, F. Y. Li, and C. Q. Jin, Solid State Commun. **148**, 538 (2008).

[4] F.-C. Hsu, J.-Y. Luo, K.-W. Yeh, T.-K. Chen, T.-W. Huang, P. M. Wu, Y.-C. Lee, Y.-L. Huang, Y.-Y. Chu, D.-C. Yan, and M.-K. Wu, Proc. Natl. Acad. Sci. U.S.A. **105**, 14262 (2008).

[5] X. Y. Zhu, F. Han, G. Mu, P. Cheng, B. Shen, B. Zeng, and H. H. Wen, Phys. Rev. B 79, 220512(R) (2009); G. F. Chen, T. L. Xia, H. X. Yang, J. Q. Li, P. Zheng, J. L. Luo, and N. L. Wang, Supercond. Sci. Technol **22**, 072001 (2009); H. Ogino, Y. Matsumura, Y. Katsura, K. Ushiyama, S. Horii, K. Kishio, and J. Shimoyama, Supercond. Sci. Technol **22**, 075008 (2009).

[6] M. K. Wu, F. C. Hsu, K. W. Yeh, T. W. Huang, J. Y. Luo, M. J. Wang, H. H. Chang, T. K. Chen, S. M. Rao, B. H. Mok, C. L. Chen, Y. L. Huang, C. T. Ke, P. M. Wu, A. M. Chang, C. T. Wu, and T. P. Perng, Physica C **469**, 340 (2009).

[7] S. Margadonna, Y. Takabayashi, Y. Ohishi, Y. Mizuguchi, Y. Takano, T. Kagayama, T. Nakagawa, M. Takata, and K. Prassides, Phys. Rev. B **80**, 064506 (2009).

[8] J.-G. Guo, S.-F. Jin, G. Wang, S.-C. Wang, K.-X. Zhu, T.-T. Zhou, M. He, and X.-L. Chen, Phys. Rev. B **82**, 180520(R) (2010).

[9] Z. G. Chen, R. H. Yuan, T. Dong, G. Xu, Y. G. Shi, P. Zheng, J. L. Luo, J. G. Guo, X. L. Chen, and N. L. Wang, Phys. Rev B **83**, 220507(R) (2011).

[10] W. Yu, L. Ma, J. B. He, D. M. Wang, T.-L. Xia, G. F. Chen, and W. Bao, Phys. Rev. Lett. **106**, 197001 (2011); H. Kotegawa, Y. Hara, H. Nohara, H. Tou, Y. Mizuguchi, H. Takeya, and Y. Takano, J. Phys. Soc. Jpn. **80**, 043708 (2011); D. A. Torchetti, M. Fu, D. C. Christensen, K. J. Nelson, T. Imai, H. C. Lei, and C. Petrovic, Phys. Rev. B **83**, 104508 (2011).

[11] T. Qian, X. P. Wang, W. C. Jin, P. Zhang, P. Richard, G. Xu, X. Dai, Z. Fang, J. G. Guo, X. L. Chen, and H. Ding, Phys. Rev. Lett. **106**, 187001(2011); Y. Zhang, L. X. Yang, M. Xu, Z. R. Ye, F. Chen, C. He, H. C. Xu, J. Jiang, B. P. Xie, J. J. Ying, X. F. Wang, X. H. Chen, J. P. Hu, M. Matsunami, S. Kimura, and D. L. Feng, Nat. Mater., **10**, 273 (2011); D. X. Mou, S. Y. Liu, X. W. Jia, J. F. He, Y. Y. Peng, L. Zhao, L. Yu, G. D. Liu, S. L. He, X. L. Dong, J. Zhang, H. D. Wang, C. H. Dong, M. H. Fang, X. Y. Wang, Q. J. Peng, Z. M. Wang, S. J. Zhang, F. Yang, Z. Y. Xu, C. T. Chen, and X. J. Zhou, Phys. Rev. Lett. **106**, 107001 (2011).

[12] A. M. Zhang, K. Liu, J. H. Xiao, J. B. He, D. M. Wang, G. F. Chen, B. Normand, and Q. M. Zhang, Phys. Rev. B **85**, 024518 (2012).

[13] Z. Wang, Y. J. Song, H. L. Shi, Z. W. Wang, Z.Chen, H. F. Tian, G. F. Chen, J. G. Guo, H. X. Yang, and J. Q. Li, Phys. Rev. B **83**, 140505(R) (2011) .

[14] W. Bao, Q. Huang, G. F. Chen, M. A. Green, D. M. Wang, J. B. He, X. Q. Wang, and Y. Qiu, Chin. Phys. Lett. **28**, 086104 (2011); F. Ye, S. Chi, Wei Bao, X. F. Wang, J. J. Ying, X. H. Chen, H. D. Wang, C. H. Dong, and Minghu Fang, Phys. Rev. Lett. **107**, 137003 (2011).

[15] R. H. Liu, X. G. Luo, M. Zhang, A. F. Wang, J. J. Ying, X. F. Wang, Y. J. Yan, Z. J. Xiang, P. Cheng, G. J. Ye, Z. Y. Li, and X. H. Chen, Europhys. Lett., **94**, 27008 (2011).

[16] D. H. Ryan, W. N. Rowan-Weetaluktuk, J. M. Cadogan, R. Hu, W. E. Straszheim, S. L. Bud'ko, and P. C. Canfield, Phys. Rev. B **83**, 104526 (2011); Z.-W. Li, X.-M. Ma, H. Pang, and F.-S. Li, unpublished (arXiv:1103.0098).

[17] A. Charnukha, J. Deisenhofer, D. Pröpper, M. Schmidt, Z. Wang, Y. Goncharov, A. N. Yaresko, V. Tsurkan, B. Keimer, A. Loidl, and A. V. Boris, Phys. Rev. B **85**, 100504(R) (2012).

[18] F. Chen, M. Xu, Q. Q. Ge, Y. Zhang, Z. R. Ye, L. X. Yang, J. Jiang, B. P. Xie, R. C. Che, M. Zhang, A. F. Wang, X. H. Chen, D. W. Shen, J. P. Hu, and D. L. Feng, Phys. Rev. X **1**, 021020 (2011).

[19] Y. Texier, J. Deisenhofer, V. Tsurkan, A. Loidl, D. S. Inosov, G. Friemel, and J. Bobroff, Phys. Rev. Lett. **108**, 237002 (2012).

[20] V. Ksenofontov, G. Wortmann, S. A. Medvedev, V. Tsurkan, J. Deisenhofer, A. Loidl, and C. Felser, Phys. Rev. B **84**, 180508(R) (2011).

[21] A. Ricci, N. Poccia, G. Campi, B. Joseph, G. Arrighetti, L. Barba, M. Reynolds, M. Burghammer, H. Takeya, Y. Mizuguchi, Y. Takano, M. Colapietro, N. L. Saini, and A. Bianconi, Phys. Rev. B **84**, 060511(R) (2011).

[22] R. H. Yuan, T. Dong, Y. J. Song, P. Zheng, G. F. Chen, J. P. Hu, J. Q. Li, and N. L. Wang, Sci. Rep. **2**, 221 (2012).

[23] W. Li, H. Ding, P. Deng, K. Chang, C. L. Song, K. He, L. Wang, X. C. Ma, J. P. Hu, X. Chen, and Q. K. Xue, Nature Phys. **8**, 126 (2012).

[24] Z. Shermadini, A. Krzton-Maziopa, M. Bendele, R. Khasanov, H. Luetkens, K. Conder, E. Pomjakushina, S. Weyeneth, V. Pomjakushin, O. Bossen, and A. Amato, Phys. Rev. Lett. **106**, 117602 (2011).

[25] G. Friemel, J. T. Park, T. A. Maier, V. Tsurkan, Y. Li, J. Deisenhofer, H.-A. Krug von Nidda, A. Loidl, A. Ivanov, B. Keimer, and D. S. Inosov, Phys. Rev. B **85**, 140511(R) (2012).

[26] A. M. Zhang, J. H. Xiao, Y. S. Li, J. B. He, D. M. Wang, G. F. Chen, B. Normand, Q. M. Zhang, and T. Xiang, Phys. Rev. B **85**, 214508 (2012).

[27] W. Bao, private communication.

[28] A. Krzton-Maziopa, Z. Shermadini, E. Pomjakushina, V. Pomjakushin, M. Bendele, A. Amato, R. Khasanov, H. Luetkens, and K. Conder, J. Phys.: Condens. Matter **23**, 052203 (2011); Y. Mizuguchi, H. Takeya, Y. Kawasaki, T. Ozaki, S. Tsuda, T. Yamaguchi, and Y. Takano, Appl. Phys. Lett. **98**, 042511 (2011); A. F. Wang, J. J. Ying, Y. J. Yan, R. H. Liu, X. G. Luo, Z. Y. Li, X. F. Wang, M. Zhang, G. J. Ye, P. Cheng, Z. J. Xiang, and X. H. Chen, Phys. Rev. B **83**, 060512 (2011); M.-H. Fang, H.-D. Wang, C.-H. Dong, Z.-J. Li, C.-M. Feng, J. Chen, and H.-Q. Yuan, Europhys Lett., **94**, 27009 (2011); J. J. Ying, X. F. Wang, X. G. Luo, A. F. Wang, M. Zhang, Y. J. Yan, Z. J. Xiang, R. H. Liu, P. Cheng, G. J. Ye, and X. H. Chen, Phys. Rev. B **83**, 212502 (2011); C.-H. Li, B. Shen, F. Han, X.-Y. Zhu, and H.-H. Wen, Phys. Rev. B **83**, 184521(2011); H.-D. Wang, C.-H. Dong, Z.-J. Li, S.-S. Zhu, Q.-H. Mao, C.-M. Feng, H.-Q. Yuan, and M.-H. Fang, Europhys. Lett. **93**, 47004 (2011).

[29] Z.-A. Ren, G.-C. Che, X.-L. Dong, J. Yang, W. Lu, W. Yi, X.-L. Shen, Z.-C. Li, L.-L. Sun, F. Zhou, and Z.-X. Zhao, Europhys. Lett. **83**, 17002 (2008); C. Wang, L.-J. Li, S. Chi, Z.-W. Zhu, Z. Ren, Y.-K. Li, Y.-T. Wang, X. Lin, Y.-K. Luo, S. Jiang, X.-F. Xu, G.-H. Cao, and Z.-A. Xu, Europhys. Lett. **83**, 67006 (2008).

[30] D. M. Wang, J. B. He, T.-L. Xia, and G. F. Chen, Phys. Rev. B **83**, 132502 (2011).

[31] W. Bao, G. N. Li, Q. Huang, G. F. Chen, J. B. He, M. A. Green, Y. Qiu, D. M. Wang, and J. L. Luo, unpublished (arXiv:1102.3674).

[32] G. Kresse and J. Hafner, Phys. Rev. B **47**, 558 (1993); G. Kresse and J. Furthmüller, Phys. Rev. B **54**, 11169 (1996).

[33] P. E. Blöchl, Phys. Rev. B **50**, 17953 (1994); G. Kresse and D. Joubert, Phys. Rev. B **59**, 1758 (1999).

[34] J. P. Perdew, K. Burke, and M. Ernzerhof. Phys. Rev. Lett. **77** 3865 (1996).

[35] K. Liu and S. Gao, Phys. Rev. Lett. **95**, 226102 (2005).

[36] Z. G. Chen, R. H. Yuan, T. Dong, G. Xu, Y. G. Shi, P. Zheng, J. L. Luo, J. G. Guo, X. L. Chen, and N. L. Wang, Phys. Rev. B **83**, 220507(R) (2011).

[37] A. P. Litvinchuk, V. G. Hadjiev, M. N. Iliev, Bing Lv, A. M. Guloy, and C. W. Chu, Phys. Rev. B **78**, 060503 (2008).

[38] X.-W. Yan, M. Gao, Z.-Y. Lu, and T. Xiang, Phys. Rev. B **83**, 233205 (2011).

[39] P. E. Sulewski, P. A. Fleury, K. B. Lyons, and S.-W. Cheong, Phys. Rev. Lett. **67**, 3864 (1991).

[40] S. Chakravarty, R. B. Laughlin, D. K. Morr, and C. Nayak, Phys. Rev. B **63**, 094503 (2001).

[41] M. Kakihana, M. Osada, M. Käll, L. Börjesson, H. Mazaki, H. Yasuoka, M. Yashima, and M. Yoshimura, Phys. Rev. B **53**, 11796 (1996).

[42] P. Zavalij, W. Bao, X. F. Wang, J. J. Ying, X. H. Chen, D. M. Wang, J. B. He, X. Q. Wang, G. F. Chen, P.-Y. Hsieh, Q. Huang, and M. A. Green, Phys. Rev. B **83**, 132509 (2011).

[43] A. Kokalj, Comp. Mater. Sci. **28**, 155 (2003). Code available from http://www.xcrysden.org/.